Harmonically bound Brownian motion in fluids under shear: Fokker-Planck and generalized Langevin descriptions

Humberto Híjar*

Grupo de Sistemas Inteligentes, Facultad de Ingeniería, Universidad La Salle, Benjamín Franklin 47, 06140, D. F., México

(Received 13 May 2014; published 27 February 2015)

We study the Brownian motion of a particle bound by a harmonic potential and immersed in a fluid with a uniform shear flow. We describe this problem first in terms of a linear Fokker-Planck equation which is solved to obtain the probability distribution function for finding the particle in a volume element of its associated phase space. We find the explicit form of this distribution in the stationary limit and use this result to show that both the equipartition law and the equation of state of the trapped particle are modified from their equilibrium form by terms increasing as the square of the imposed shear rate. Subsequently, we propose an alternative description of this problem in terms of a generalized Langevin equation that takes into account the effects of hydrodynamic correlations and sound propagation on the dynamics of the trapped particle. We show that these effects produce significant changes, manifested as long-time tails and resonant peaks, in the equilibrium and nonequilibrium correlation functions for the velocity of the Brownian particle. We implement numerical simulations based on molecular dynamics and multiparticle collision dynamics, and observe a very good quantitative agreement between the predictions of the model and the numerical results, thus suggesting that this kind of numerical simulations could be used as complement of current experimental techniques.

DOI: 10.1103/PhysRevE.91.022139 PACS number(s): 05.40.Jc, 05.70.Ln, 36.20.Ey, 03.65.Ge

I. INTRODUCTION

Systems driven outside thermodynamic equilibrium by the action of external forces appear in almost every phenomenon observed in nature, experiments, and industrial processes. They use to exhibit exclusive features not present when the same systems are in equilibrium [1,2]. Good examples of such special features are the existence of long-ranged fluctuations in fluids kept in nonequilibrium stationary states [3], and the formation of patterns induced by instabilities in systems far from equilibrium [4]. Generalizations of thermodynamics based on the assumption of local equilibrium have been proposed along the years which have been very successful in describing situations close to equilibrium [5]. However, theoretical models for systems far from equilibrium can not be obtained straightforwardly from equilibrium theories because the usual thermodynamic variables are in general insufficient for characterizing the driven states [4].

One of such nonequilibrium problems that has received considerable attention during the last decades concerns the statistical mechanics description of Brownian motion in sheared fluids [6], as a representative of systems driven from equilibrium by externally imposed flows. Indeed, a Brownian particle (BP) immersed in an inhomogeneous flow represents one of the simplest full-solvable models of a system coupled to a nonequilibrium bath in which the effects of the external gradient on the thermodynamic and transport properties can be analytically tracked down to a significant extent. This has been done from diverse standpoints ranging from kinetic theory [7,8], Fokker-Planck and Langevin equations [9,10], and mesoscopic nonequilibrium thermodynamics [11–13]. In addition, Brownian motion in a shear flow has been proved to be amenable for experimental [14–17] and numerical [18–20] work.

In the presence of shear, the pressure tensor of an ensemble of independent BPs has been suggested to be modified by contributions increasing as the square of the velocity gradient [10]. This result is related with the existence of the so-called nonequilibrium equations of state (NEEOS), which are generalizations of the classical relations between thermodynamic variables for systems in nonequilibrium steady states [21]. Pressure and energy NEEOS have been studied for systems with a stationary heat flux from extended irreversible thermodynamics [4], and for fluids in steady shear flow from molecular dynamics (MD) simulations [21–23].

Another related nonequilibrium model consists of a BP immersed in an inhomogeneous flow and simultaneously subjected to a harmonic central force. The effects of harmonic forces on Brownian motion in flowing fluids were first considered several years ago in Ref. [24], where attention was focused in showing that the introduction of harmonic constraints might lead to a sufficiently fast decay of the velocity correlation function of the BP that ensures the existence of a long-time diffusion behavior in external Couette and Poiseuille flows. The problem of harmonically constrained Brownian dynamics in sheared solvents has recovered relevance due to the recent advances in experimental techniques based on optical tweezers that allow for manipulation of individual microsized particles, as well as for observation of their trajectories. A recent fundamental experimental study [25] has shown that the external imposition of shear breaks down the spatial symmetry and the time reversibility of the dynamics of the trapped particle, an effect that was already predicted to exist for free BPs moving in a sheared fluid [10]. This feature was quantified in terms of the correlation functions for displacements of the BP along the directions of shear and increasing velocity, which possess exclusive nonequilibrium asymmetric time-irreversible contributions. The experimental results were justified in terms of models based on Langevin and Smoluchowski equations [25,26]. Asymmetric time-irreversible correlations have been predicted to exist also

*humberto.hijar@lasallistas.org.mx

in the problem of tracking control of individual colloidal particles through nonhomogeneous flows [27]. In this case, the nonequilibrium effects have been observed by means of simulations based on MD and multiparticle collision dynamics (MPC).

The simple Langevin description, which is based on the classical Stokes' formula for the drag force experienced by a particle moving in a viscous fluid, has been also extended to consider the effects of backflow on the dynamics of a harmonically bound BP. Hydrodynamic correlations in the surrounding fluid transported by shear and longitudinal wave propagation have been shown to have a strong influence in the dynamics of the trapped BP. They induce a slow decay in the correlation functions for velocities of the BP taking the form of long-time tails [28] and, more strikingly, they produce resonant peaks in the corresponding correlation functions for displacements [29], which strongly contrast with the overdamped dynamics expected from the simple Langevin description. Although this latter fundamental result has been verified by experimental and simulation techniques [29], its observation was restricted to the case of harmonically bound Brownian motion in a quiescent solvent.

In this paper, we will extend the analysis carried out in Refs. [24–29] in diverse ways. First, in Sec. II we will revisit the Langevin model for harmonically bound Brownian motion in fluids under shear and construct the corresponding Fokker-Planck equation (FPE). The solution of the latter will be explicitly derived yielding the probability distribution function (PDF) for observing specific values of the position and velocity of the BP. We consider that this extension is relevant as long as it shows that the PDF for a harmonically bound particle describing Brownian motion in sheared baths, already obtained in Ref. [26], can be also derived as the solution of the complementary approach based on a proper boundary-value problem. Subsequently, we will use the derived PDF to calculate, in the stationary limit, the average energy and the pressure of the particle harmonically trapped in the nonequilibrated bath. This will yield a NEEOS [Eq. (12)] and an expression for the equipartition law [Eq. (15)], both of which differ from their equilibrium forms by terms increasing as the square of the imposed shear. These results could be significant since they exhibit that the effect of the external shear on the thermodynamic properties of the confined particle can be quite large indeed. Afterwards, we will extend the proposed model to include the effects of hydrodynamic viscous correlations and compressibility on the nonequilibrium dynamics of the harmonically bound BP under shear. With this purpose, we will use a generalized Langevin equation (GLE) where the frequency-dependent drag force will be modeled by the corresponding Faxén theorem for unsteady motion in compressible fluids with sheared flow [30]. These effects will be estimated in terms of the correlation functions for the velocities of the bound BP, which are time irreversible and asymmetric as well, but exhibit strong deviations from the behavior predicted by the simple Langevin-Fokker-Planck model. Specifically, we will show that the nonequilibrium terms of the correlation functions indeed present long-time tails and resonances induced by hydrodynamic backflow. According to our model, the long-time tails of the nonequilibrium correlations are expected to have the same exponent found in the equilibrium case. On the other hand, resonance in the nonequilibrium correlation functions depends on the externally imposed shear, which can be used to enhance the strength of the resonant peaks.

In Sec. III, we will describe the implementation of a simulation method, combining MD and MPC, designed to study the dynamics of the BP confined in the harmonic trap and the nonequilibrium environment from an independent approach. In Sec. IV, we will present a comparison between the analytical and the numerical results. We will verify that models based on Langevin and Fokker-Planck dynamics exhibit the same qualitative behavior concerning the PDFs, the NEEOS, and the dynamic correlation functions. However, a complete quantitative correspondence for the latter will be achieved only if viscous and sound propagation effects are taken into account. Finally, in Sec. V we will summarize our conclusions and discuss the limitations of our analysis.

II. HARMONIC BROWNIAN MOTION UNDER STEADY SHEAR

A. Fokker-Planck description

In this section, we will study the motion of a spherical BP of mass M and radius R, immersed in an incompressible Newtonian fluid which is in a nonequilibrium stationary state induced by a uniform shear. We will write the velocity field of the fluid unperturbed by the BP in the form of a plane Couette flow, namely, $\vec{v}\,(\vec{r}\,) = \vec{v}\,(0) + \mathbf{Z}\cdot\vec{r}$, where $\vec{v}\,(0)$ denotes the velocity field at the origin, $\mathbf{Z}$ is the uniform velocity gradient tensor, and $\vec{r}$ is the position vector.

We will introduce now a Langevin model to describe the time evolution of the BP, under the assumptions that its dynamics occur at a time scale much larger than that corresponding to the fluctuations of the surrounding fluid and that the friction term can be modeled by the Faxén theorem for the motion of a sphere through a viscous fluid in an inhomogeneous stationary flow [31]. We will also consider an external force which is meant to constrain harmonically the motion of the BP around a fixed position in space $\vec{r}_0$, $\vec{F} = -k\,(\vec{x} - \vec{r}_0)$, where $\vec{x}$ denotes the position of the BP, and k is the restoring coefficient of the trap. These assumptions yield the following evolution equation for the position of the BP relative to $\vec{r}_0$, $\vec{X} = \vec{x} - \vec{r}_0$:

$$\frac{d^2\vec{X}}{dt^2} + \beta\frac{d\vec{X}}{dt} + \left[\omega_0^2\mathbf{1} - \beta\mathbf{Z}\right]\cdot\vec{X} - \beta\vec{v}\,(\vec{r}_0) = \vec{\mathcal{A}}, \qquad (1)$$

where we have written the result in terms of the damping ratio $\beta = \gamma/M$, with γ the drag coefficient; the natural frequency of the trap $\omega_0 = \sqrt{k/M}$; the unit matrix $\mathbf{1}$; and the stochastic force per unit mass $\vec{\mathcal{A}}$.

Then, it can be noticed that Eq. (1) is equivalent to a set of three stochastic damped oscillators asymmetrically coupled by the velocity gradient tensor $\mathbf{Z}$. The last term on the left-hand side of Eq. (1) tilts the harmonic potential in the direction of the velocity field at the position of the harmonic trap. An extensive characterization of the stochastic dynamics of the trapped BP was provided in Refs. [25,26] in terms of a similar Langevin equation. Here, we will present the complementary approach of deriving the phase-space PDF for the trapped particle from the FPE associated to Eq. (1).

This FPE can be obtained by following the usual procedure of considering the increments of $\vec{X}$ and its time derivative $\vec{U} = d\vec{X}/dt$, occurring during a time interval δt, which is considered long compared to the periods of the stochastic accelerations but short compared to the intervals in which any of the physical parameters change appreciably. We thus have $\delta\vec{X} = \vec{U}\delta t$, and $\delta\vec{U} = -[\beta\vec{U} + (\omega_0^2\mathbf{1} - \beta\mathbf{Z})\cdot\vec{X}]\delta t + \vec{B}(\delta t)$, where $\vec{B}$ is the net stochastic acceleration suffered by the BP in the time interval δt. The statistical properties of $\vec{B}$ will be assumed to correspond to a Gaussian-Markov process. Thus, the probability for observing an acceleration $\vec{B}$ will be written as

$$w(\vec{B}) = \frac{1}{(4\pi q\delta t)^{3/2}\,(\det\boldsymbol{\Omega})^{3/2}} e^{-\vec{B}^{\mathrm{T}}\cdot\boldsymbol{\Omega}\cdot\vec{B}/4q\delta t}, \tag{2}$$

where $q = \beta k_B T/M$, with k_B the Boltzmann constant and T the temperature of the bath; $\boldsymbol{\Omega}$ is a dimensionless matrix that measures the strength of the correlations existing between the components of the stochastic forces; and the superscript T indicates the transpose of the corresponding matrix or vector. Due to time-reversal invariance, $\boldsymbol{\Omega}$ must be symmetric and for a solvent with a uniform flow we simply have $\boldsymbol{\Omega} = \mathbf{1}$. The imposition of an external shear introduces contributions into the elements of $\boldsymbol{\Omega}$ outside the main diagonal. However, these nonequilibrium contributions are expected to be small [26].

Since the process is of the Markov type, the probability distribution in phase space $W(\vec{X},\vec{U},t)$ can be obtained from the probability distribution at earlier times $W(\vec{X},\vec{U},t-\delta t)$ and the transition probability in velocity space $\Psi(\vec{X},\vec{U};\delta\vec{U})$ through

$$\begin{aligned} &W(\vec{X}+\vec{U}\delta t,\vec{U},t+\delta t) \\ &\quad = \int d(\delta\vec{U})\, W(\vec{X},\vec{U}-\delta\vec{U},t)\Psi(\vec{X},\vec{U}-\delta\vec{U};\delta\vec{U}). \end{aligned} \tag{3}$$

The transition probability Ψ is directly obtained from the Gaussian assumption (2), and by expanding the diverse involved functions in a Taylor series and taking the limit $\delta t \to 0$, the FPE obeyed by W is found to be

$$\begin{aligned} \frac{\partial W}{\partial t} &= -\vec{\nabla}_{\vec{X}}\cdot(W\vec{U}) \\ &\quad + \vec{\nabla}_{\vec{U}}\cdot\left\{W\left[\beta(\vec{U}-\vec{v}(\vec{r}_0)) + \left(\omega_0^2\mathbf{1}-\beta\mathbf{Z}\right)\cdot\vec{X}\right]\right\} \\ &\quad + \frac{\beta k_B T}{M}\vec{\nabla}_{\vec{U}}\vec{\nabla}_{\vec{U}}:(W\boldsymbol{\Omega}), \end{aligned} \tag{4}$$

where $\vec{\nabla}_{\vec{X}}$ and $\vec{\nabla}_{\vec{U}}$ denote the differential operators in $\vec{X}$ and $\vec{U}$ spaces, respectively.

The solution of this equation is derived in Appendix A. Here, it will be cast in the form

$$W(\vec{X},\vec{U};t) = \frac{\exp\left\{-\frac{1}{2}\begin{pmatrix}\vec{X}-\vec{X}_{\mathrm{d}}\\ \vec{U}-\vec{U}_{\mathrm{d}}\end{pmatrix}^{\mathrm{T}}\cdot\mathbf{H}^{-1}\cdot\begin{pmatrix}\vec{X}-\vec{X}_{\mathrm{d}}\\ \vec{U}-\vec{U}_{\mathrm{d}}\end{pmatrix}\right\}}{(2\pi)^3(\det\mathbf{H})^{1/2}}, \tag{5}$$

where the covariance matrix $\mathbf{H} = \mathbf{H}(t)$ is defined through Eqs. (A9)–(A14), while $\vec{X}_{\mathrm{d}} = \vec{X}_{\mathrm{d}}(t)$ and $\vec{U}_{\mathrm{d}} = \vec{U}_{\mathrm{d}}(t)$ are the first moments of the distribution W, i.e., the deterministic part of the formal solution of the Langevin equation (1). For concreteness, we will restrict ourselves to consider only stationary flows sheared along the $\hat{e}_3$ axis, whose velocity increases linearly along the $\hat{e}_1$ direction, for a usual Cartesian reference frame with unit vectors $\{\hat{e}_1,\hat{e}_2,\hat{e}_3\}$. Thus, $\mathbf{Z}$ will take the following explicit form:

$$\mathbf{Z} = \begin{pmatrix} 0 & 0 & 0 \\ 0 & 0 & 0 \\ \dot{\gamma} & 0 & 0 \end{pmatrix}, \tag{6}$$

where $\dot{\gamma}$ is the magnitude of the velocity gradient. In this case, functions $\vec{X}_{\mathrm{d}}$ and $\vec{U}_{\mathrm{d}}$ take the form given by Eqs. (A15)–(A17).

It can be observed by inspection of Eqs. (5) and (A9)–(A17) that the FPE approach yields, as it should, the same PDF previously derived from the Langevin description in Ref. [26], as long as both methods are based on the assumption that the underlying stochastic forces on the BP are of the Gaussian-Markov type.

The PDF function given by Eqs. (5) and (A9)–(A17) contains all the effects produced by the nonequilibrium bath on the statistical properties of the harmonically bound BP. These equations show that the PDF for this particle is a Gaussian, as in the equilibrium case, but anisotropic due to the presence of the external shear.

With the purpose of performing a subsequent validation of the result of our molecular simulations, we will summarize here the main effects that the imposed flow has on the distribution W in the important case where correlations between stochastic forces are not significantly modified by the external flow, i.e., when $\boldsymbol{\Omega} = \mathbf{1}$. In this case, and considering the asymptotic limiting behavior of the functions defining the PDF, it follows that the reduced probability of observing the velocities components U_1 and U_3 at large times is given by

$$\begin{aligned} W(U_1,U_3) &= \frac{M}{2\pi k_B T\sqrt{1+\dot{\gamma}^2/2\omega^2}} \\ &\quad \times \exp\left\{-\frac{M}{2k_B T}\left[U_1^2 + \frac{U_3^2}{1+\dot{\gamma}^2/2\omega^2}\right]\right\}. \end{aligned} \tag{7}$$

On the other hand, the asymptotic reduced probability for the BP to be found around a position vector with coordinates X_1 and X_3 reads as

$$\begin{aligned} W(X_1,X_3) &= \frac{1}{\sqrt{4\pi^2\det\mathbf{G}}}\exp\left\{-\frac{1}{2}\left(X_1, X_3 - \frac{\beta}{\omega^2}v_3(\vec{r}_0)\right)\right. \\ &\quad \left.\cdot\mathbf{G}\cdot\begin{pmatrix} X_1 \\ X_3 - \frac{\beta}{\omega^2}v_3(\vec{r}_0)\end{pmatrix}\right\}, \end{aligned} \tag{8}$$

where the matrix $\mathbf{G}$ is given by

$$\begin{aligned} \mathbf{G} &= \frac{k}{k_B T[4\omega^4 + \dot{\gamma}^2(\beta^2+2\omega^2)]} \\ &\quad \times \begin{pmatrix} 4\omega^4 + 2\dot{\gamma}^2(\beta^2+\omega^2) & -2\beta\dot{\gamma}\omega^2 \\ -2\beta\dot{\gamma}\omega^2 & 4\omega^4 \end{pmatrix}. \end{aligned} \tag{9}$$

These results show that the net effect of the external shear on the distribution of velocities consists in extending it along the direction of the imposed flow, while in the direction of the velocity gradient the distribution is not modified and remains the equilibrium Maxwell distribution. In addition, the imposed shear distorts the distribution of positions from its equilibrium form in such a way that its width in the

direction of the velocity gradient decreases, while its width along the direction of shear increases. In addition, it can be observed that the axis representing the maximum elongation of the nonequilibrium distribution $W(X_1, X_3)$ turns out to be rotated with respect to the Cartesian direction $\hat{e}_3$, by an amount approximately proportional to $\dot{\gamma}$, an effect that was noticed first in Refs. [25,26].

B. Nonequilibrium equation of state and average energy

In this section we will use the previous calculation of the nonequilibrium PDF in order to derive expressions for the pressure and the average energy of the harmonically bound BP in the sheared bath. For this purpose, we will consider the distribution described by Eqs. (5) and (A9)–(A17) in the stationary limit.

We start by noticing that the proper pair of thermodynamic conjugate variables for representing the state of particles trapped in harmonic potentials are the so-called harmonic volume $\mathcal{V}$ and harmonic pressure $\mathcal{P}$ [32]. The former is a measure of the effective space occupied by the oscillator and, in thermal equilibrium at a given temperature, it is defined as the extensive variable ω_0^{-3} since the oscillator moves within a volume of the order of $(k_BT/M\omega_0^2)^{3/2}$. On other hand, the harmonic pressure represents the net opposition that the particle presents against the external harmonic force, and guarantees the achievement of mechanical equilibrium. It is defined as $\mathcal{P} = \mathrm{Tr}\bar{\boldsymbol{\sigma}}/3$, where the average stress tensor $\bar{\boldsymbol{\sigma}}$ is given analogously to the corresponding quantity in elasticity theory [33]

$$\bar{\boldsymbol{\sigma}} = \frac{1}{\mathcal{V}} \int_V dV \boldsymbol{\sigma}, \tag{10}$$

where normalization is considered with respect to the harmonic volume.

Operationally, the harmonic pressure can be calculated directly as the average of the harmonic potential over the reduced PDF for observing the BP around a given position $\vec{X}$, $W(\vec{X})$. More precisely [32],

$$\mathcal{P} = \frac{2}{3\mathcal{V}} \int d\vec{X}\, W(\vec{X}) \frac{k}{2} \vec{X} \cdot \vec{X}. \tag{11}$$

The function $W(\vec{X})$ can be obtained in the stationary limit from Eqs. (5) and (A9)–(A17), and the average involved in Eq. (11) can be straightforwardly performed yielding

$$\mathcal{P} = \frac{k_BT}{\mathcal{V}} \left(1 + \dot{\gamma}^2 \frac{\omega_0^2 + \beta^2}{6\omega_0^4}\right). \tag{12}$$

Equation (12) reveals that the imposed velocity gradient indeed modifies the mathematical relationship existing between the thermodynamic variables $\mathcal{P}$, $\mathcal{V}$, and T, which results in a NEEOS for the harmonically bound BP in a sheared bath.

It must be stressed at this point that the externally imposed shear modifies not only the harmonic pressure, but the harmonic volume as well, by expanding the effective space occupied by the BP, as it has been discussed previously in the context of Eqs. (8) and (9). This effect will be shown to be significant subsequently in Sec. IV A and, thus, it is important to estimate it. With this purpose, let us consider the average over the stationary reduced PDF $W(\vec{X})$, of the dyad product $\vec{X}\vec{X}$, which is found to be

$$\langle \vec{X}\vec{X} \rangle = \int d\vec{X}\, W(\vec{X}) \vec{X}\vec{X} = \frac{k_BT}{k} \begin{pmatrix} 1 & 0 & \frac{\dot{\gamma}\beta}{2\omega_0^2} \\ 0 & 1 & 0 \\ \frac{\dot{\gamma}\beta}{2\omega_0^2} & 0 & \left[1 + \dot{\gamma}^2 \frac{\omega_0^2 + \beta^2}{2\omega_0^4}\right] \end{pmatrix}. \tag{13}$$

The effective volume occupied by the BP can be calculated similarly to the equilibrium case by first rotating the coordinate system to the set of principal axes of the previous matrix, and multiplying the resulting harmonic lengths along the new directions [34] or, equivalently, by taking the square root of the (invariant) determinant of the matrix on the right-hand side of Eq. (13), and multiplying the result times $(M/k_BT)^{3/2}$. Both procedures yield

$$\mathcal{V} = \frac{1}{\omega_0^3} \left(1 + \dot{\gamma}^2 \frac{2\omega_0^2 + \beta^2}{4\omega_0^2}\right)^{\frac{1}{2}}, \tag{14}$$

which exhibits the changes in the harmonic volume induced by the external shear $\dot{\gamma}$.

Finally, notice that Eq. (13) can be used to calculate the average potential energy of the harmonic oscillator in the simple shear flow $k\langle \vec{X} \cdot \vec{X} \rangle/2$, while in order to calculate its average kinetic energy we must obviously consider the average $M\langle \vec{U} \cdot \vec{U} \rangle/2$, which can be obtained from the stationary nonequilibrium PDF derived from Eqs. (5) and (A9)–(A17). Adding the resulting expressions for these averages we obtain the total mean energy, namely,

$$\langle E \rangle = 3k_BT \left(1 + \dot{\gamma}^2 \frac{2\omega_0^2 + \beta^2}{4\omega_0^4}\right), \tag{15}$$

which can be cast in the form of the classical (equilibrium) equipartition theorem $\langle E \rangle = 3k_BT_{\mathrm{eff}}$, with an effective temperature rescaled by the shear rate $T_{\mathrm{eff}} = T(1 + \dot{\gamma}^2 \frac{2\omega_0^2 + \beta^2}{4\omega_0^4})$. This result can be interpreted as if the net effect of nonequilibrium sheared bath was to supply the BP with an additional amount of energy that increases the strength of its thermal motion with respect to the equilibrium situation.

C. Hydrodynamic vorticity and sound propagation effects

The simple model for Brownian motion based on the Langevin equation (1) or, equivalently, on the FPE [Eq. (4)], is known to be incomplete to describe the dynamics of actual microsized objects in dilute solution. This is especially the case if the dynamics of the suspended particles is observed at short time scales, where large deviations from the simple Langevin picture arise from the development of hydrodynamic correlations in the form of viscous vortex formation and sound propagation due to finite compressibility of the solvent [35]. These mechanisms contribute to a friction force on the BP that acquires different values at different stages of its motion, an effect that can be modeled by using a time-dependent friction term in the Langevin description [2]. For the harmonically bound BP, this procedure yields a stochastic equation that in

Fourier space can be cast in the form

$$-i\omega\vec{U}(\omega) = -\omega_0^2\,\vec{X}(\omega) + \frac{1}{M}\vec{K}(\omega) + \vec{\mathcal{A}}(\omega), \tag{16}$$

where we have assumed, for simplicity, that the center of the harmonic trap is located at a position $\vec{r}_0$ such that $\vec{v}(\vec{r}_0) = 0$; and $\vec{K}(\omega)$ is precisely the now frequency-dependent friction force.

Expressions for $\vec{K}(\omega)$ have been proposed since a long time ago that consider viscous [36,37] and compressibility effects [38], as well as diverse degrees of slip on the surface of the suspended particle, particles with different geometries, and particles in arbitrary flow conditions (see, e.g., Refs. [30,31,39–42]). In the analysis to be performed in this section, $\vec{K}(\omega)$ will be obtained from the generalized Faxén's theorem for unsteady motion through a compressible fluid [Eq. (3.14) in Ref. [30]]. This expression gives the friction force for a spherical particle in an arbitrary time-dependent flow subjected to nonslip boundary conditions. For the special case of motion in a steady plane Couette flow, it can be shown that this general result yields

$$\vec{K}(\omega) = -M\tilde{\beta}(\omega)\vec{U}(\omega) + M\tilde{\tilde{\beta}}(\omega)\mathbf{Z}\cdot\vec{X}(\omega), \tag{17}$$

where, for brevity, the definitions of the auxiliary functions $\tilde{\beta}(\omega)$ and $\tilde{\tilde{\beta}}(\omega)$ are given in Appendix B [see Eqs. (B1) and (B2)]. It is interesting to notice that by replacing Eq. (17) into Eq. (16) and taking the inverse Fourier transform, we obtain

$$\begin{aligned}\frac{d\vec{U}}{dt} &= -\int_{-\infty}^{t} d\xi\,\tilde{\beta}(t-\xi)\vec{U}(\xi)\\ &\quad -\int_{-\infty}^{t} d\xi\left[\omega_0^2\delta(t-\xi)\mathbf{1} - \tilde{\tilde{\beta}}(t-\xi)\mathbf{Z}\right]\cdot\vec{X}(\xi) + \vec{\mathcal{A}}(t),\end{aligned} \tag{18}$$

which has the form of a GLE with a retarded friction coefficient $\tilde{\beta}(t)$ [2], where $\delta(\dots)$ represents the Dirac delta function. Equation (18) shows that retardation is also present in the nonequilibrium coupling induced by the external shear $\mathbf{Z}$. This is a consequence of the fact that in the generalized Faxén's theorem friction depends, through a memory kernel, on the surface and volume averages of the fluid's velocity.

In order to study systematically the effects of hydrodynamic momentum transport in the dynamics of the trapped BP in sheared flows, we will analyze the behavior of its dynamic correlation functions. In this paper, we shall focus our attention in correlation functions for velocities. This could be an interesting case since, as far as we know, although these functions have been calculated for the special case of simple Langevin dynamics, they have not been measured yet in actual experiments [26]. Our calculation will be subsequently compared with the results of numerical experiments where these correlation functions are indeed accessible.

Correlation functions will be calculated under the assumption that the statistical properties of the stochastic forces acting on the BP are identical to those observed in the equilibrium case. Consequently, $\vec{\mathcal{A}}$ will be considered to have zero mean

$$\langle\vec{\mathcal{A}}(\omega)\rangle = 0, \tag{19}$$

where $\langle\dots\rangle$ denotes the stochastic average; and to obey the generalized fluctuation-dissipation relation

$$\langle\vec{\mathcal{A}}(\omega')\vec{\mathcal{A}}(\omega)\rangle = \frac{4\pi k_B T}{M}\mathrm{Re}\{\tilde{\beta}(\omega)\}\delta(\omega'+\omega)\,\mathbf{1}, \tag{20}$$

which fulfills the condition that the proper velocity distribution in thermal equilibrium is achieved [2]. Notice that in Eq. (20) we have neglected cross correlations between stochastic forces that could arise as a consequence of the imposed shear. In addition, we have introduced the notation $\mathrm{Re}\{\dots\}$ to indicate the real part of a complex variable.

Correlation functions between the components of the velocity vector can be calculated by replacing Eq. (17) into Eq. (16), using the relation $\vec{U}(\omega) = -i\omega\vec{X}(\omega)$, and solving for the function $\vec{U}(\omega)$. Then, after evaluating the result at two different frequencies, averaging according to Eq. (20), and inverting the Fourier transformation, we obtain

$$\begin{aligned}&\langle\vec{U}(t+\tau)\vec{U}(t)\rangle\\ &= \frac{k_B T}{\pi M}\int_{-\infty}^{\infty} d\omega\, e^{i\omega\tau}\frac{\omega^2\mathrm{Re}\{\tilde{\beta}(\omega)\}}{|m(\omega)|^4}[|m(\omega)|^2\mathbf{1}\\ &\quad + m^*(\omega)\tilde{\tilde{\beta}}(\omega)\mathbf{Z}^{\mathrm{T}} + m(\omega)\tilde{\tilde{\beta}}^*(\omega)\mathbf{Z} + |\tilde{\tilde{\beta}}(\omega)|^2\mathbf{Z}\cdot\mathbf{Z}^{\mathrm{T}}],\end{aligned} \tag{21}$$

where * indicates complex conjugate and the function $m(\omega)$ is defined by $m(\omega) = \omega_0^2 - \omega^2 - i\omega\tilde{\beta}(\omega)$.

Equation (21) contains the effects of the nonequilibrium state on the solvent on the correlation matrix for velocities through those terms involving the matrix $\mathbf{Z}$. It shows that $\dot{\gamma}$ breaks down the spatial symmetry of the dynamics of the Brownian oscillator. Specifically, the autocorrelation function in the direction of shear $\hat{e}_3$ becomes higher than the corresponding correlation in the direction of the velocity gradient $\hat{e}_1$ due to the term proportional to the square of the velocity gradient $\mathbf{Z}\cdot\mathbf{Z}^{\mathrm{T}}$. More strikingly, cross correlations along these directions, which vanish in harmonic Brownian motion in a fluid at rest, become visible in the nonequilibrium case, increasing linearly as function of $\mathbf{Z}$. Furthermore, it can be observed from Eq. (21) that these cross correlations do not have the same time dependence and, consequently, it is found that $\mathbf{Z}$ breaks also the time reversibility in the dynamics of the harmonic BP. These features are shared with those noticed first in Refs. [10,26] for Brownian motion in external incompressible shear flows.

Notice that in Appendix B functions $\tilde{\beta}$ and $\tilde{\tilde{\beta}}$ have been defined in terms of the characteristic times $\tau_s = R/c$ and $\tau_f = R^2/\nu$, where c and ν are the velocity of sound propagation and the kinematic viscosity of the solvent, respectively. Times τ_s and τ_f define the scales where compressibility and viscous effects are expected to manifest [35]. Vorticity and compressibility effects could be neglected in the limit of small values of both τ_f and τ_s, meaning that viscous momentum diffusion and sound propagation occur too fast that they are unable to perturb the motion of the particle at the Brownian time scale $\tau_B \sim \beta^{-1}$ [43]. In this limit, both functions $\tilde{\beta}$ and $\tilde{\tilde{\beta}}$ reduce to β, the dynamics reduces to the simple Langevin case, and explicit expressions for the elements of the correlation matrix can be found by performing the corresponding integrals in the complex plane. Specifically,

this procedure yields the expressions presented below for the elements of the correlation matrix, which will be split in an equilibrium contribution independent of the externally imposed shear, plus a nonequilibrium contribution depending on **Z**. The equilibrium elements, hereafter denoted by the superscript eq, have the classical form [44]

$$\langle U_i(t+\tau)U_j(t)\rangle^{\rm eq} = \frac{k_{\rm B}T}{M(\mu_1-\mu_2)}[\mu_1 e^{\mu_1\tau} - \mu_2 e^{\mu_2\tau}]\delta_{ij}, \tag{22}$$

where the time difference τ is considered positive.

On the other hand, the only nonvanishing nonequilibrium elements of the correlation matrix, from now on represented by the superscript neq, are found to be

$$\langle U_1(t+\tau)U_3(t)\rangle^{\rm neq} = -\frac{k_BT}{2M(\mu_1-\mu_2)}\dot\gamma(e^{\mu_1\tau} - e^{\mu_2\tau}), \tag{23}$$

$$\langle U_3(t+\tau)U_1(t)\rangle^{\rm neq} = \frac{k_BT}{2M(\mu_1-\mu_2)}\dot\gamma\left\{\left[1+2\left(\frac{\mu_1+\mu_2}{\mu_1-\mu_2}\right)^2 - 2\mu_1\tau\frac{\mu_1+\mu_2}{\mu_1-\mu_2}\right]e^{\mu_1\tau}\right.$$
$$\left. -\left[1+2\left(\frac{\mu_1+\mu_2}{\mu_1-\mu_2}\right)^2 - 2\mu_2\tau\frac{\mu_1+\mu_2}{\mu_2-\mu_1}\right]e^{\mu_2\tau}\right\}, \tag{24}$$

and

$$\langle U_3(t+\tau)U_3(t)\rangle^{\rm neq} = \frac{k_BT}{M}\frac{\dot\gamma^2}{2(\mu_1-\mu_2)^3}\left[-\frac{\mu_1^2(3-\mu_1\tau)+\mu_2^2(1+\mu_1\tau)}{\mu_1}e^{\mu_1\tau} + \frac{\mu_2^2(3-\mu_2\tau)+\mu_1^2(1+\mu_2\tau)}{\mu_2}e^{\mu_2\tau}\right]. \tag{25}$$

Corrections induced by compressibility and viscous momentum transfer to the correlation functions given by Eqs. (22)–(25) can be inferred by replacing Eqs. (B1) and (B2) into Eq. (21) and performing the resulting integrals numerically. We follow this procedure and illustrate in Figs. 1 and 2 the comparison between the correlations obtained from simple Langevin dynamics and those obtained from the generalized scheme. There, we consider correlations normalized with respect to their maximum value at equilibrium $Y_{ij} = M\langle\langle U_i(t+\tau)U_j(t)\rangle\rangle/k_BT$, as functions of the dimensionless time difference $\bar\tau = \tau\beta/2$. Curves in Figs. 1 and 2 were obtained for the specific values $\tau_{\rm f} = \tau_{\rm B}$ and $\tau_{\rm s} = \tau_{\rm f}/2$, while the external shear normalized with respect to the relaxation time was chosen to be $\dot\gamma/\beta = 0.2$. For harmonically bound Brownian motion, another relevant characteristic time scale is defined by the trap relaxation time $\tau_{\rm K} = \gamma/k$, which was fixed at the value $\tau_{\rm K} = 12.5\tau_{\rm B}$. These parameters were chosen

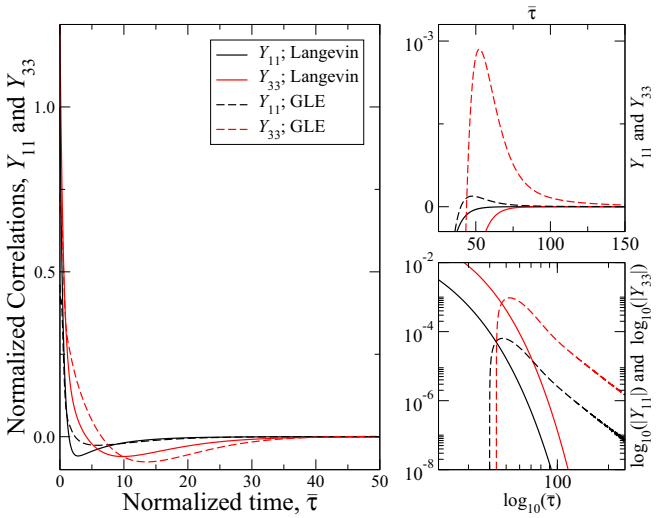

FIG. 1. (Color online) Normalized autocorrelation functions for velocities of a harmonically bound BP in a stationary Couette flow. Y_{11} corresponds to BP's velocities projected in the direction of the external velocity gradient, while Y_{33} corresponds to the velocities along the direction of the external shear. Two cases are considered for correlations obtained from the simple Langevin model yielding Eqs. (23)–(25) (Langevin); and from the model based on the GLE [Eq. (18)] (GLE). The specific values used to obtain these curves are described through the text.

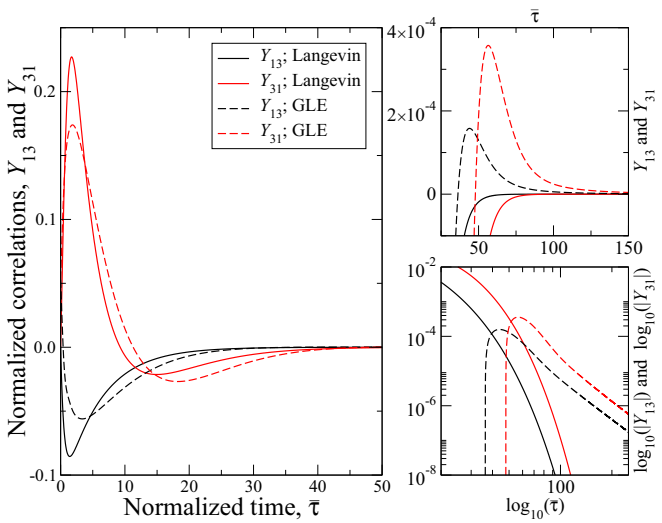

FIG. 2. (Color online) The same as in Fig. 1 for the normalized cross correlations Y_{13} and Y_{31}.

just for illustrative purposes, but satisfy the typical relation $\tau_s < \tau_f \lesssim \tau_B < \tau_K$, found in experimental situations.

It can be noticed first that for the two models considered in Figs. 1 and 2, based on simple Langevin dynamics and on the GLE, the imposed shear breaks indeed the symmetry in the correlation functions as it was discussed in the paragraphs following Eq. (21).

It can be also observed that due to hydrodynamic effects correlations functions for the velocities of the bound BP exhibit an interesting behavior differing in several respects from the one predicted by simple Langevin dynamics. First, they extend over longer periods of time than those expected from the Langevin model. Actually, the detailed analysis of the curves presented in the $\log_{10}$-$\log_{10}$ insets at the right bottom corner of Figs. 1 and 2 shows that, indeed, retardation in viscous resistance due to viscosity and compressibility induces slow decay of the correlation functions in the form of long-time tails. This behavior is similar to the one that has been confirmed to exist for free Brownian motion in equilibrium fluids [28,37–42]. The present analysis shows that long-time tails prevail in nonequilibrium conditions. Moreover, the decaying exponent for the equilibrium correlation Y_{11} is the same as that corresponding to the nonequilibrium correlations Y_{13}, Y_{31}, and Y_{33}.

Another interesting effect derived from the generalized Langevin scheme is shown in the insets at the right top corner of Figs. 1 and 2, where it can be observed that while correlations derived from the simple Langevin model vanish asymptotically, those obtained from the generalized description exhibit a resonant peak as a consequence of hydrodynamic memory. This effect is the counterpart in velocity space of the resonances observed recently in correlations of displacements of harmonically trapped BPs in equilibrium fluids [29]. Figures 1 and 2 illustrate that the resonant effect persists in nonequilibrium correlations. Moreover, it turns out that the nonequilibrium character of the solvent enhances the intensity of the effect by amplifying the height of the peak.

In the following section, we will discuss the implementation of a numerical method that will allow us to simulate the dynamics of a BP in a plane Couette flow, subjected to an external harmonic force. This will eventually lead us to the observation of the predicted behavior of the correlation functions discussed here.

III. SIMULATION METHOD

A. Hybrid MD-MPC algorithm

We performed numerical experiments in order to observe the effects produced by the externally imposed shear on the dynamics of the harmonically bound BP. Our implementation consisted of a hybrid algorithm combining MD [45], which was used to describe the evolution of the system at the microscopic time scale, and MPC [46,47], that allowed us to incorporate thermal fluctuations and hydrodynamic effects. Both MD and MPC are particle-based methods and their coupling is used in simulations as a bridge that spans the two widely separated characteristic time scales occurring in Brownian motion. Our implementation is quite similar to the one used previously in the study of tracking control of colloidal particles in stationary flows [27]. For brevity, details about our methodology will not be presented here but can be found in that reference.

We considered N fluid particles of mass m, and a single BP of mass M, moving in a cubic simulation box of volume L^3. Solvent particles were assumed to be point particles and in order to achieve their coupling with the BP, an explicit interaction force was introduced between the former and the latter. This force was derived from the Weeks-Chandler-Andersen potential [Eq. (47) in Ref. [27]], with interaction strength ϵ and effective diameter σ. The system evolved in time in a succession of propagation and collision steps. Propagation steps were carried out at short-time intervals of size $\Delta t_{\rm MD}$, while collision steps took place only at regular, larger periods of time of size $\Delta t > \Delta t_{\rm MD}$. In a propagation step, the positions and velocities of all the particles in the system were advanced by applying the velocity-Verlet update algorithm [45]. At the regular periods of time of size Δt, the simulation box was subdivided in smaller cells of volume a^3, where it was applied the original collision rule for MPC, known as stochastic rotation dynamics [48–50]. Thus, the center of mass velocity was calculated for every cell and the particles located within the same cell were forced to change their velocities according to

$$\vec{u}_i'(t) = \vec{u}_{\rm c.m.}(t) + \mathbf{R}(\alpha;\hat{e}) \cdot [\vec{u}_i(t) - \vec{u}_{\rm c.m.}(t)], \qquad (26)$$

where $\vec{u}_{\rm c.m.}$ is the center of mass velocity of the cell where the ith particle is located and $\mathbf{R}(\alpha;\hat{e})$ is a stochastic matrix for a rotation by a fixed angle α, around the axis $\hat{e}$, which was chosen for each collision cell by selecting a point on the surface of a sphere from a uniform probability distribution. We applied a homogeneous displacement of the MPC cells by a vector with random components uniformly distributed in-between $-a/2$ and $a/2$, before the collision took place, in order to guarantee the Galilean invariance of the method [51,52].

In Fig. 3, we present a schematic illustration of the simulated system, where the three Cartesian directions are shown. For this reference frame we used periodic boundary conditions along the x_2 and x_3 directions, and Lees-Edwards boundary

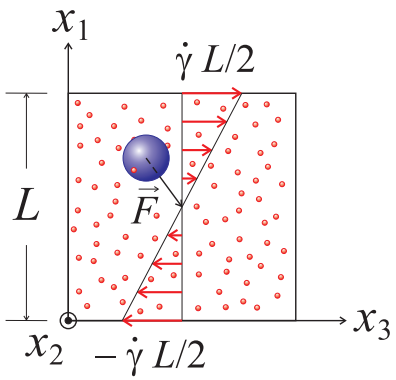

FIG. 3. (Color online) Schematic illustration of the simulated system. The BP is represented by a big blue sphere, while solvent particles are represented by small red spheres. The application of LEBC, as it is described in the text, establishes the planar Couette flow represented by the red arrows. The harmonic force on the BP, $\vec{F}$, is directed towards the center of the simulation box.

conditions (LEBC) [53] along the x_1 direction in order to drive the system to a nonequilibrium state characterized by the linear velocity profile $\vec{v}\,(\vec{r}) = -\dot{\gamma}\,L/2\,\hat{e}_3 + \mathbf{Z}\cdot\vec{r}$, which is also shown schematically in Fig. 3.

In order to prevent viscous heating of the MPC fluid [49,54,55], we incorporated into our algorithm a thermostatting step in which velocities of the particles located within the same cell were rescaled after the collision step [Eqs. (53) and (54) in Ref. [27]]. Finally, a momentum reset step was also incorporated after the thermostatting procedure, in order to prevent net flow of the solvent caused by the momentum transfer from the trapped particle to the MPC fluid [Eq. (55) in Ref. [27]].

Our simulations started with particles placed in the box at random positions and velocities obtained from uniform distributions. The total momentum of the system was fixed to zero, and its total energy was fixed to the value of the equipartition law at the temperature of the thermostat. Then, the hybrid MD-MPC algorithm was applied over a sufficiently long-time period in order to guarantee that the proper distribution of velocities and hydrodynamic fields were established. The harmonic restoring force was applied with $\vec{r}_0$ located at the center of the simulation box, as it is schematically shown in Fig. 3. The position and velocity vectors of the BP were stored as functions of the simulation time in order to calculate subsequently their statistical properties.

IV. RESULTS

A. Nonequilibrium probability distribution functions

In order to validate our numerical implementation, we performed first simulations of a BP subjected to a harmonic force field in a fluid at rest. We decided to fix the simulation parameters at $m = 1$, $k_BT = 1$, $a = 1$, $\alpha = 135^\circ$, $\Delta t = 0.1$, $\epsilon = 2.5\,k_BT$, $\sigma = 2a$, $\Delta t_{\rm MD} = \Delta t/200$, and $M = 200\,m$, where simulation units rather than physical units will be used from now on. Finally, the size of the simulation box was fixed at $L = 20\,a$, and the number of MPC particles per cell at $n_0 = 3$.

It has been discussed in Ref. [27] that for this choice of parameters no instabilities are expected for the MD algorithm and that the Brownian dynamics is expected to behave close to the Markovian description [48]. Moreover, the effective friction coefficient for the BP was calculated for this numerical setup and it was found to be $\gamma = 48.9 \pm 1.6$. We considered the dynamics of the bound BP in the overdamped regime by choosing the value $k = 1.0$, for the restoring coefficient of the trap. A detailed analysis of the Brownian motion carried out by particles in sheared fluids and confined in harmonic traps in the critically damped and underdamped regimes can be found in Ref. [56].

The simulation scheme described in Sec. III was followed by allowing the system to thermalize in a total of 2×10^6 simulation steps of the hybrid MD-MPC algorithm. Afterwards, we recorded the position and the velocity of the BP at regular time intervals of size $25\,\Delta t_{\rm MD}$ during a simulation extending over 1×10^8 steps. We used the resulting time series to measure directly the PDFs $W(U_1,U_3)$ and $W(X_1,X_3)$ of the harmonically bound BP in the equilibrated solvent. These results can be directly compared with the two-dimensional equilibrium distributions obtained from Eqs. (7)–(9) in the limit $\dot{\gamma} = 0$. In Figs. 4 and 5, we present such comparison. It can be observed that the analytical and numerical results show a very good agreement, although in the case of the distribution $W(X_1,X_3)$, presented in Fig. 5, the numerical results exhibit strong irregularities due to an insufficient statistical sampling of values of $\vec{X}$.

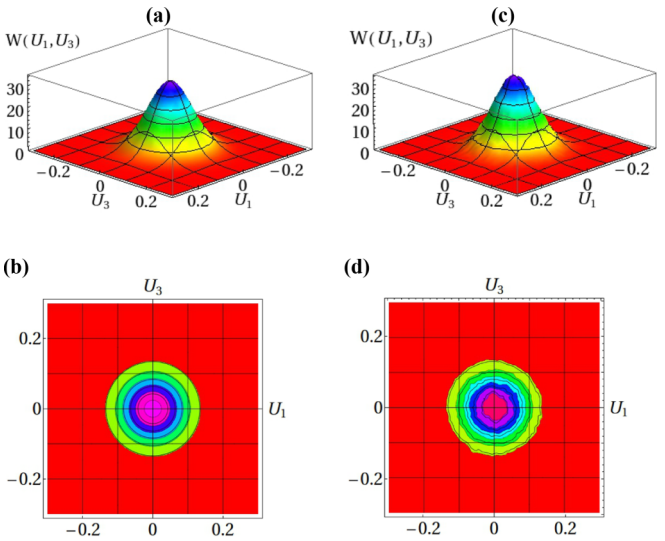

FIG. 4. (Color online) Probability distribution functions for the velocities U_1 and U_3 of a harmonically bound BP in an equilibrium environment. Case (a) is obtained analytically from Eq. (7) with $\dot{\gamma} = 0$, and case (b) represents the corresponding analytical level curves. Case (c) is obtained independently from the simulation method combining MD and MPC described in Sec. III, and case (d) illustrates the corresponding numerical level curves.

Then, we performed numerical experiments for harmonic Brownian motion in fluids under plane Couette flows with different values of the velocity gradient. Our nonequilibrium simulations were executed by allowing systems to thermalize again in 2×10^6 steps of the MD-MPC algorithm, but

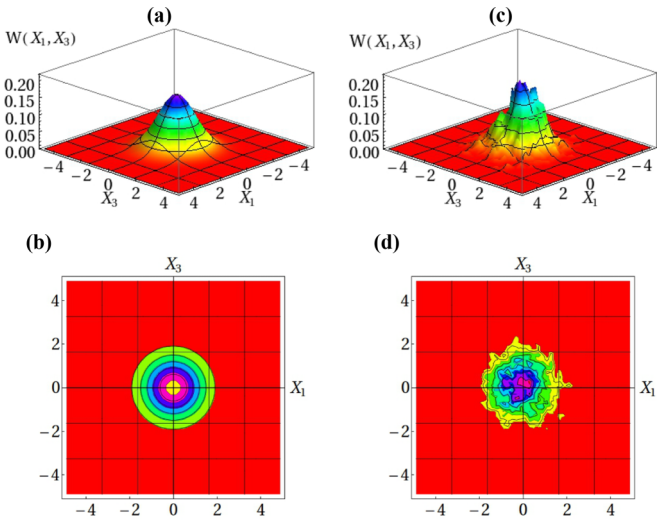

FIG. 5. (Color online) The same as in Fig. 4 for the PDF of the coordinates X_1 and X_3 of the BP.

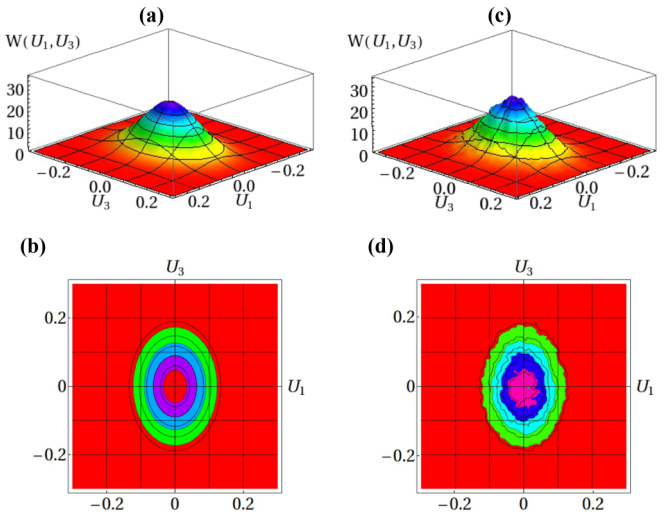

FIG. 6. (Color online) Probability distribution function for the velocities U_1 and U_3 of the harmonically bound BP coupled to a nonequilibrium fluid with velocity gradient $\dot{\gamma} = 0.1$. Cases (a) and (b) were obtained analytically from Eq. (7), while cases (c) and (d) were obtained independently from the simulation method combining MD and MPC described in Sec. III.

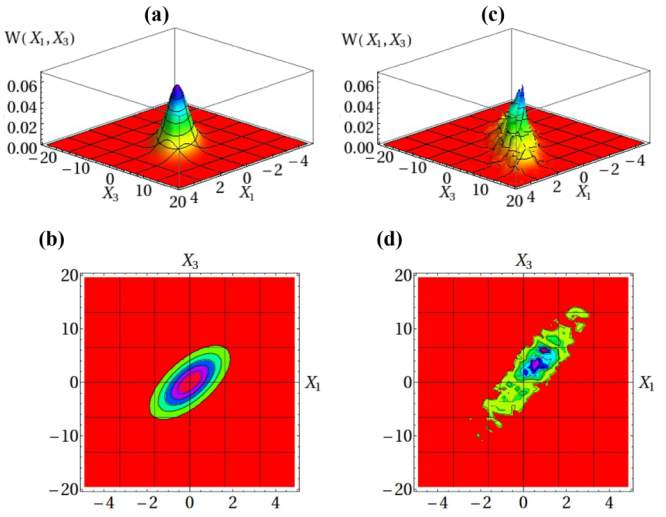

FIG. 7. (Color online) The same as in Fig. 6 for the nonequilibrium PDF of the coordinates X_1 and X_3 of the harmonically bound BP.

extending in time over 5×10^7 simulation steps, i.e., one half of the length of the corresponding equilibrium simulations. Once again, time series were generated in which observations of $\vec{X}$ and $\vec{U}$ at regular time intervals of size $25\Delta t_{\mathrm{MD}}$ were stored, and used to estimate the corresponding nonequilibrium PDFs. The velocity PDF $W(U_1,U_3)$ obtained in numerical experiments is compared in Fig. 6 with its analytical counterpart as expressed by Eq. (7), for the particular case of a shear with magnitude $\dot{\gamma} = 0.1$. Notice that for this value of $\dot{\gamma}$ the Stokes number $\mathcal{S} = \dot{\gamma}/\beta$, characterizing the deviation from equilibrium in terms of the BP's dynamics [10,27], becomes $\mathcal{S} = 0.4$. This value of $\mathcal{S}$ is one order of magnitude smaller than those considered in the study of Brownian motion in shear flow in the absence of harmonic constraints [10].

It can be observed in Fig. 6 that the analytical and numerical distributions are very similar and that a very good agreement between simulations and theory is once again obtained. The surfaces and level curves represented in Fig. 6 should be also compared with those appearing in Fig. 4, corresponding to the equilibrium case.

In Fig. 7, we present the corresponding nonequilibrium PDF for positions $W(X_1,X_3)$, obtained analytically from Eqs. (8) and (9), and numerically from our simulation experiments using $\dot{\gamma} = 0.1$. A comparison of the scales appearing in Figs. 5 and 7 shows that the range of values in which X_1 and X_3 can be found is significantly increased by the action of the external gradient. Therefore, the deficiency in the statistical sampling of the position of the BP already noticed in Fig. 5 has more drastic consequences in the nonequilibrium case and the collected data are insufficient to generate a well defined experimental surface. Nevertheless, it can be appreciated that the numerical PDF $W(X_1,X_3)$ exhibits the qualitative behavior predicted by the model based on the FPE (4).

B. Harmonic pressure, harmonic volume, and average energy

We have discussed in Sec. II B in the context of the simple model based on the FPE (4) that the imposition of the external shear is expected to modify the harmonic volume, the equation of state, and the equipartition law of the harmonically bound BP. In order to observe this effect, we performed eight numerical experiments in which the harmonically trapped BP was simulated to be in the presence of diverse plane Couette flows with shear rates uniformly distributed in the interval $\dot{\gamma} = [0,0.07]$. The estimations of $\mathcal{V}$, $\mathcal{P}$, and $\langle E \rangle$ were obtained by using the averages of the dyad matrices $\vec{X}\vec{X}$ and $\vec{U}\vec{U}$, calculated from the experimental time series of $\vec{X}(t)$ and $\vec{U}(t)$.

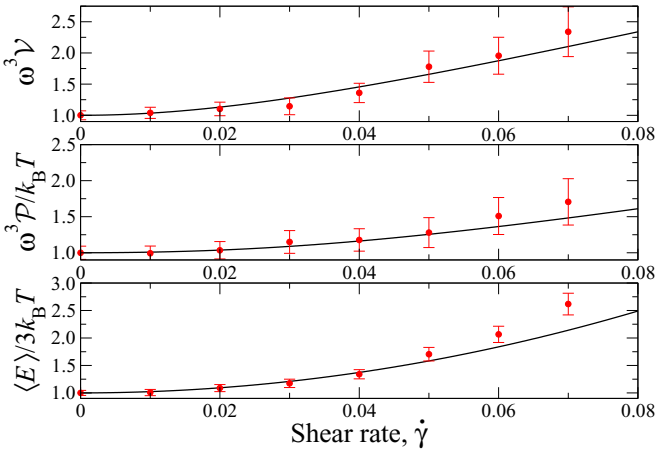

FIG. 8. (Color online) Normalized harmonic volume $\omega^3\mathcal{V}$, harmonic pressure $\omega^3\mathcal{P}/k_BT$, and total energy $\langle E \rangle/3k_BT$ of a harmonically bound BP in shear flows with different shear rates $\dot{\gamma}$. Continuous curves correspond to Eqs. (14), (12), and (15), for comparison of harmonic volume, harmonic pressure, and energy, respectively. The results obtained from the numerical experiments are represented by the symbols with error bars.

We present in Fig. 8 the normalized numerical estimations of the harmonic volume, the harmonic pressure, and the total energy as function of the external shear. There, we compare the numerical results with the analytical expressions derived in Sec. II B, Eqs. (12), (14), and (15). We observe a very good agreement between the theoretical and numerical approaches for small values of the external shear $\dot{\gamma} \leqslant 0.5$, while for larger values of $\dot{\gamma}$ the numerical estimations are found to be larger than the theoretical predictions. This discrepancy arises from the fact that for large values of $\dot{\gamma}$, we have not achieved a good estimation of the PDF for displacements of the BP, as it was discussed at the end of Sec. IV A. In addition, it should be remembered that Eqs. (12), (14), and (15) were obtained under the assumption that the stochastic forces are not modified by the imposed shear, which implied $\Omega = \mathbf{1}$ in Eqs. (7)–(9). However, for large values of $\dot{\gamma}$, this condition is expected to be invalid and the nonequilibrium part of the matrix Ω should modify the form of the stationary PDFs (7)–(9). In turn, this will produce a different dependence of $\mathcal{P}$, $\mathcal{V}$, and $\langle E \rangle$ on $\dot{\gamma}$, as it is manifested in the results presented in Fig. 8 for $\dot{\gamma} \gtrsim 0.5$.

C. Velocity correlation functions

We carried out the measurement of the two-time correlation matrix for velocities $\langle \vec{U}(t+\tau)\vec{U}(t)\rangle$ by using the time series of the velocity vector recorded during the simulation stage. For brevity, we will discuss here only the representative case corresponding to simulations in an external shear flow with velocity gradient $\dot{\gamma} = 0.05$. The elements of the correlation matrix were estimated according to the usual formula

$$\langle U_i(t+\tau)\, U_j(t)\rangle \simeq \frac{1}{\mathcal{N}_\tau}\sum_{l=1}^{\mathcal{N}_\tau} U_i(t_l+\tau)\, U_j(t_l)\,, \qquad (27)$$

where the index l runs over the recorded values of the time series, and $\mathcal{N}_\tau$ is the total data available to perform the average for a given time difference τ. We will describe our results in terms of the normalized correlations Y_{ij}, introduced in Sec. II C. In the experimental case, functions Y_{ij} were obtained from the correlations given by Eq. (27) divided by the maximum value of the autocorrelation function $\langle U_1(t+\tau)\, U_1(t)\rangle$.

The experimental correlation functions will be compared with those predicted by the simple Langevin model [Eqs. (22)–(25)] and by the scheme based on the GLE including compressibility and vorticity effects. However, some points are worth mentioning before we proceed to such comparison. First, it should be stressed that when the generalized Langevin model defined by Eq. (16) is supplemented with Eqs. (17), (B1), and (B2), it is assumed that stick boundary conditions are valid on the surface of the BP. In contrast, our simulation scheme based on purely repulsive interactions between the BP and the fluid particles corresponds better to slip boundary conditions [27,57]. Thus, Eqs. (17), (B1), and (B2) are not applicable for describing the results of our simulations. Instead, we should use a proper expression for the frequency dependent drag force experienced by a spherical particle moving through a viscous compressible fluid with slip boundary conditions. Unfortunately, although such expression exists for motion in a fluid at rest [39,42,58], as far as we know, the corresponding equation containing the effects of stationary inhomogeneous flow has not been reported in the literature. Therefore, we propose here a modification of our model by assuming the size of the BP to be small, in such a way that the drag force on it can be considered to depend only on its relative velocity with respect to the local unperturbed velocity field [43], i.e., $\vec{K} = -M\beta[d\vec{x}/dt - \vec{v}(\vec{x})] = -M\beta(\vec{U} - \mathbf{Z}\cdot\vec{X})$. Thus, the frequency dependent drag force is proposed to be $\vec{K}(\omega) = -M\beta_{\rm slip}(\omega)[\vec{U}(\omega) - \mathbf{Z}\cdot\vec{X}(\omega)]$, instead of that one given by Eq. (17). The function $\beta_{\rm slip}(\omega)$ has been obtained in Ref. [58], and for simplicity we present its explicit form in Appendix B [see Eq. (B3)], where a new characteristic time has been introduced $\tau_{\rm d} = D_l/c^2$, with D_l the longitudinal kinematic viscosity of the solvent. By replacing the new expression for the drag force in Eq. (16) and following the same procedure used in Sec. II C, we obtain now

$$\begin{aligned}\langle \vec{U}(t+\tau)\vec{U}(t)\rangle = \frac{k_B T}{\pi M}\int_{-\infty}^{\infty} d\omega\, e^{i\omega\tau}\,\frac{\omega^2 \mathrm{Re}\{\beta_{\rm slip}(\omega)\}}{|m(\omega)|^4} \\ \times\,[|m(\omega)|^2\mathbf{1} + m^*(\omega)\beta_{\rm slip}(\omega)\mathbf{Z}^{\rm T} \\ + m(\omega)\beta^*_{\rm slip}(\omega)\mathbf{Z} + |\beta_{\rm slip}(\omega)|^2\mathbf{Z}\cdot\mathbf{Z}^{\rm T}],\end{aligned} \qquad (28)$$

instead of Eq. (21). Notice that in Eq. (28), $m(\omega)$ is defined as $m(\omega) = \omega_0^2 - \omega^2 - i\omega\beta_{\rm slip}(\omega)$.

Equations (28) and (B3) will be the expressions used to perform the comparison with the simulation results. In this procedure, we will use the value for the drag coefficient in the Langevin description $\beta = \gamma/M = 0.245 \pm 0.008$, previously estimated in Ref. [27]. On the other hand, the quantities $\tau_{\rm s}$, $\tau_{\rm f}$, and $\tau_{\rm d}$ will be considered to be effective parameters that can be selected to improve the correspondence between the model and the simulation results.

We consider first the experimental correlation function $Y_{11}(\bar{\tau})$, and its fits obtained from the simple Langevin model (22), and from the numerical solution of the GLE (28) with $\mathbf{Z} = 0$. We obtain the estimations of the characteristic times $\tau_{\rm s}$, $\tau_{\rm f}$, and $\tau_{\rm d}$ by means of a steepest descent method that minimizes the difference between the experimental results and the theoretical prediction. From this procedure we obtain the values $\tau_{\rm s} = 0.01$, $\tau_{\rm f} = 1.03$, and $\tau_{\rm d} = 0.41$. The comparison between the experimental correlation and those obtained from the simple and generalized Langevin schemes is shown in Fig. 9, where it can be observed that the generalized model fits better the simulation results than the model based on simple Langevin dynamics. The correspondence between the simulations and the theoretical results obtained from the GLE is shown to be better at short times.

The same set of parameters β, $\tau_{\rm s}$, $\tau_{\rm f}$, and $\tau_{\rm d}$, obtained according to the procedure described in the preceding paragraph, was subsequently used to calculate the correlation functions $Y_{13}(\bar{\tau})$, $Y_{31}(\bar{\tau})$, and $Y_{33}(\bar{\tau})$, expected to exhibit the strongest nonequilibrium effects. We calculated these functions again from the simple Langevin model yielding Eqs. (23)–(25), and from the numerical solution of Eq. (28) corresponding to the generalized scheme. The analytical curves are compared with the results of numerical simulations in Fig. 10, where it can be observed that although both schemes can be used to describe correctly the qualitative behavior of the velocity correlation

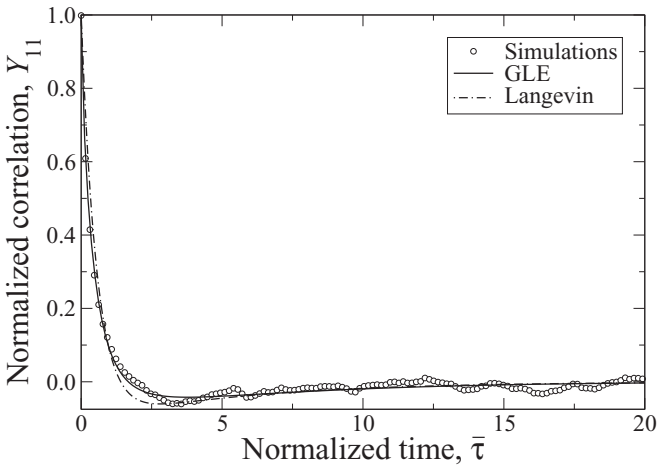

FIG. 9. Normalized correlation Y_{11} as function of the normalized time difference $\bar{\tau}$. The result obtained from simulations (symbols) are compared against the fits obtained from the generalized Langevin scheme (continuous curve) and the simple Langevin description (dotted dashed curve).

functions, the model based on the GLE is in general better to achieve a quantitative agreement with the numerical results.

The differences between the GLE model and the numerical results observed in Fig. 10 are similar to those that will be found in the following section. Consequently, we will postpone a discussion about them until that point.

D. Nonequilibrium resonant peaks

Finally, we performed a series of simulations designed to observe the resonance effect induced by hydrodynamic backflow in the nonequilibrium velocity correlation functions. It should be stressed that this effect is expected to be significant only when the time scale of the harmonic trap τ_K is similar to the viscous relaxation time τ_f, i.e., when $\tau_K \sim \tau_f$ [29]. Therefore, with the purpose of reducing the difference between these time scales, we performed simulations modifying the following parameters with respect to those introduced in Sec. IV A: $\Delta t = 0.05$ and $n_0 = 5$. Notice that this modification is intended to increase the collisional viscosity of the MPC solvent, thus reducing the value of τ_f. We also extended the size of the simulated system to $L = 24\,a$, in order to reduce possible finite size effects.

For this selection of parameters we performed nonequilibrium simulations with $\dot{\gamma} = 0.3$, and found that the damping ratio of the BP was $\beta \simeq 0.635$. This allowed us to increase the stiffness of the harmonic trap up to $k = 20$, in order to bring τ_K close to τ_f. Notice that for this value of k, the dynamics of the harmonically bound BP was still overdamped but simulations were performed very close to the critically damped regime.

We conducted a first nonequilibrium experiment in which the time series for $\vec{U}(t)$ was recorded at regular time intervals along a simulation extending over 2.5×10^7 MD-MPC steps after thermalization. We calculated the correlation functions using this time series and found that the resonant peaks, if any, should be located in the region where statistical noise becomes significant. Therefore, in order to reduce the strength of this noise, we performed a total of 56 independent nonequilibrium experiments having the same extension in time as the one mentioned previously. We calculated the correlation functions for each one of these experiments, and obtained the final estimation by averaging over the whole set of independent measurements. The result of this procedure is illustrated in Fig. 11, where we have used curves with filled symbols to represent our normalized numerical correlations. We noticed that for the selected set of simulation parameters, the correlation functions $Y_{11}(\bar{\tau})$, $Y_{31}(\bar{\tau})$, and $Y_{33}(\bar{\tau})$ still approach to zero in the noisy region of the time domain, where they take values of the same order of magnitude than the statistical noise. This is illustrated in the insets of Fig. 11 for the special case of the autocorrelation Y_{11}. Therefore, it would be difficult to assert that the resonant peaks in these correlations have been indeed observed. However, it can be also noticed in Fig. 11 that the nonequilibrium correlation function $Y_{13}(\bar{\tau})$ approaches to zero earlier, in the region where noise is not so large. The insets on the right hand side of Fig. 11 show that,

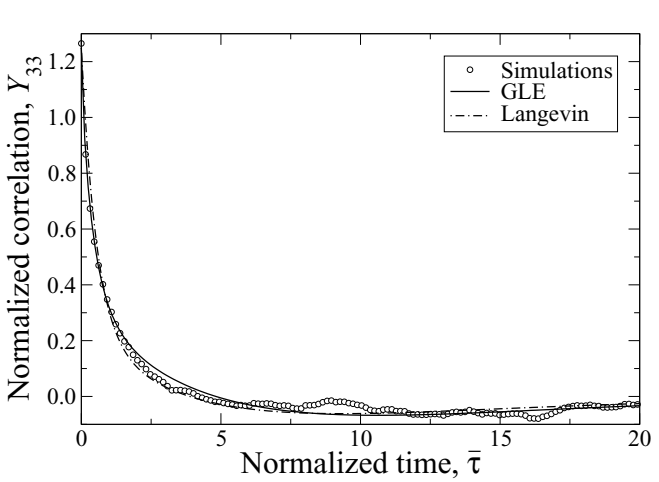

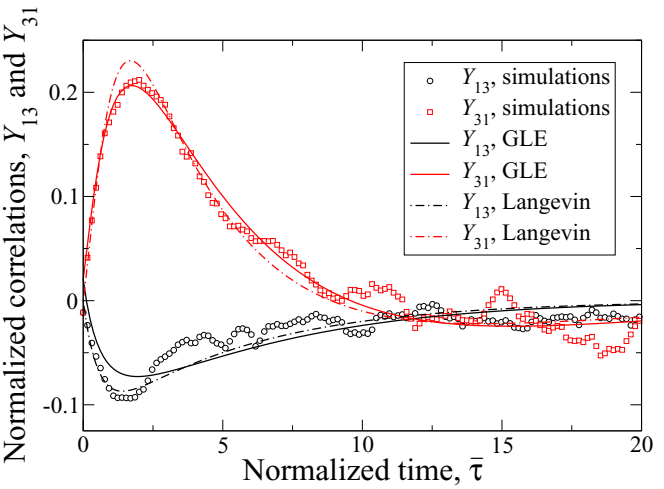

FIG. 10. (Color online) Normalized correlations Y_{33}, Y_{13}, and Y_{31} as function of the normalized time difference $\bar{\tau}$ for a harmonically bound BP in a solvent with a plane Couette flow with shear rate $\dot{\gamma} = 0.05$. Symbols represent the results of simulations, continuous curves the approximations based on the generalized Langevin model, and dotted dashed curves the fits obtained from simple Langevin dynamics.

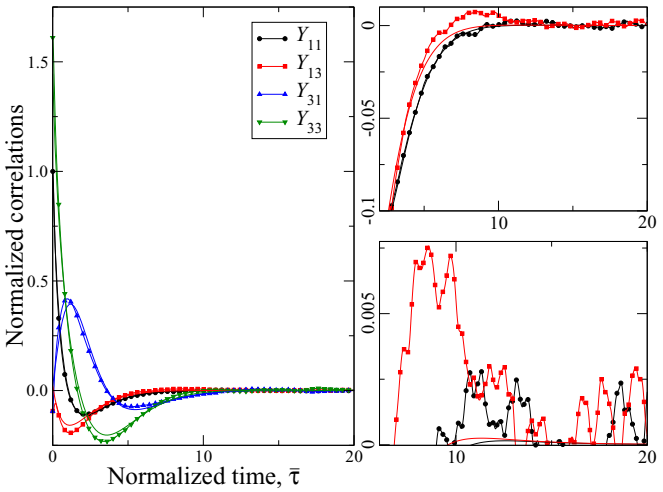

FIG. 11. (Color online) Normalized correlations for a harmonically bound BP in a solvent with a uniform shear rate $\dot{\gamma} = 0.3$. Curves with filled symbols represent the results of simulations, while continuous curves were obtained from Eqs. (28) and (B3). The specific parameters used to obtain both the experimental and analytical curves are described through Sec. IV D. The insets at the right hand side show that the cross correlation Y_{13} has a resonant peak whose height is larger than the strength of the statistical noise.

at least for this correlation function, a resonant peak can be identified having a height that is considerably larger than the strength of the noise.

We have also illustrated in Fig. 11, by means of continuous curves, the fit of the experimental data obtained from the generalized Langevin scheme, Eqs. (28) and (B3). In order to simplify the present analysis in these equations, we have neglected the contribution of compressibility by making $\tau_s = 0$, as well as the contribution of the characteristic time τ_D. On the other hand, τ_f was estimated by following the optimization scheme described in Sec. IV C, from which we obtained the value $\tau_f = 0.0929$. It can be observed that there is a very good quantitative agreement between the theoretical model and the simulation results in the case of the normalized correlation $Y_{11}(\bar{\tau})$. However, correlations Y_{13}, Y_{31}, and Y_{33} exhibit clear deviations from the analytical results, similar to those that can be observed in Figs. 9 and 10 in Sec. IV C. In particular, it can be observed that the model based on the GLE seems to give a poor estimation of the heights of the resonant peaks.

We consider that these discrepancies arise from the simplifications performed in deriving Eq. (28), in particular, from the assumption that the fluctuation matrix $\mathbf{\Omega}$ is independent of the external shear. Actually, in shear flows the nondiagonal elements of $\mathbf{\Omega}$ do not vanish and depend on the shear rate [25,59]. As a consequence, for large values of the velocity gradient, the behavior of the correlation functions could be expected to be different from the one predicted by Eq. (28). For instance, if the nondiagonal elements of $\mathbf{\Omega}$ were different from zero, cross correlation functions would be modified due to the presence of a term with the form $m(\omega)\, m^*(\omega)\, \mathbf{\Omega}$, inside the brackets of the integrand in Eq. (28). Similarly, the autocorrelation in the direction of flow would be modified by the presence of the terms $m^*(\omega)\, \beta_{\rm slip}(\omega)\, \mathbf{Z} \cdot \mathbf{\Omega}$ and $m(\omega)\, \beta^*_{\rm slip}(\omega)\, \mathbf{\Omega} \cdot \mathbf{Z}^{\rm T}$, appearing within the same brackets. Under the assumption of a linear relation between $\mathbf{\Omega}$ and $\dot{\gamma}$, these contributions would not modify the dependence of Y_{13}, Y_{31}, and Y_{33} on $\dot{\gamma}$. However, they would induce a different frequency dependence and, consequently, would change the way in which these functions depend on t.

V. CONCLUSIONS

We have studied the Brownian motion of a particle confined in a harmonic trap and a nonequilibrium environment subjected to a simple shear flow. First, we have derived the FPE describing the stochastic motion of such particle and obtained its solution in detail, yielding the nonequilibrium PDF for observing the BP around a given point in its configuration space. We have confirmed that this PDF is the same as the one derived previously in Ref. [25] from simple Langevin dynamics. Thus, we have introduced here the approach based on the solution of a boundary value problem which serves as a complement to the description founded in stochastic differential equations that has been used up to now to deal with the present problem. We have used the solution of the FPE equation to calculate the harmonic pressure and the total energy of the harmonically bound BP, and found that both quantities are strongly modified as a consequence of the external shear. On the one hand, the NEEOS [Eq. (12)] is modified from its equilibrium form by a term increasing as the square of the external shear. On the other hand, the nonequilibrium bath has the net effect of increasing the strength of the thermal random motion of the harmonically trapped BP, whose average energy can be written in the form of the classical equipartition law [Eq. (15)], but with an effective nonequilibrium temperature depending on the square of the external shear.

In addition, we have introduced an extension of the simple Langevin (Fokker-Planck) model that incorporates hydrodynamic viscosity and sound propagation effects by means of a generalized equation with a time-dependent friction force. We have found that hydrodynamic memory produces strong modifications in the nonequilibrium part of the velocity correlations of the trapped BP, as compared with those predicted from the simple Langevin scheme. In particular, as a result of hydrodynamic backflow, the nonequilibrium correlation functions develop long-time tails and resonant peaks, similar to those exhibited by correlation functions in equilibrium [29]. One of the main results of this work was to notice that the external shear may produce an enhancement of the resonant peaks, as it is illustrated in Fig. 1. This effect suggests that it should be possible to use a nonequilibrium mechanism to adjust the height of the hydrodynamic resonances.

Subsequently, we have implemented hybrid MD-MPC simulations that allowed us to verify some of the results derived from the theoretical models. For small values of the external shear, the numerical results were found to exhibit the behavior predicted by the simple Langevin model concerning the nonequilibrium PDF, the NEEOS, and the average energy of the particle. Thus, it was found that this model could be very useful to describe the statistical properties of the trapped BP in the stationary limit and close to equilibrium situations.

It must be also emphasized that the used numerical technique naturally incorporated hydrodynamic vorticity and

sound propagation effects, a property that allowed us to observe the role that these mechanisms play in the stochastic dynamics of the BP. In particular, we have shown that the description of the equilibrium and nonequilibrium velocity correlation functions can be significantly improved when such effects are taken into account. Furthermore, we were able to confirm the existence of the resonant peaks predicted by the generalized model in the nonequilibrium cross correlation function $\langle U_1(t+\tau)\,U_3(t)\rangle$, where subindexes 1 and 3 indicate the directions of increasing velocity and flow, respectively.

The analysis carried out in this paper could be improved by relaxing the performed assumption that the statistical properties of the stochastic forces are independent of the shear rate. Finally, it should be mentioned that in this work we have not studied the behavior of the correlation functions for displacements of the trapped BP under shear. A calculation of the nonequilibrium and hydrodynamic memory effects on these functions is currently under research, as well as a detailed analysis of the enhancement of the resonances induced by the external shear on both the velocity and displacement correlations.

ACKNOWLEDGMENTS

H.H. thanks Universidad La Salle for financial support under Grant No. I-062/12, is a Fellow of SNI, Mexico, and thanks J. Fernández from Universidad La Salle for his help with Figs. 4-7.

APPENDIX A: SOLUTION OF THE FPE (4)

In order to find the solution of the FPE (4), we propose to recast it in terms of the sixfold vector $\vec{\Gamma}^{\mathrm{T}} = \{[-\beta\vec{v}(\vec{r}_0) + (\omega^2\mathbf{1} - \beta\mathbf{Z})\cdot\vec{X}]^{\mathrm{T}}, \vec{U}^{\mathrm{T}}\}$, a procedure that yields

$$\frac{\partial W}{\partial t} = -\vec{\nabla}_{\vec{\Gamma}}\cdot(\mathbf{A}\cdot\vec{\Gamma}W) - \vec{\nabla}_{\vec{\Gamma}}\cdot(\mathbf{B}\cdot\vec{\nabla}_{\vec{\Gamma}}W), \tag{A1}$$

where the matrices $\mathbf{A}$ and $\mathbf{B}$ have the following explicit form defined by blocks:

$$\mathbf{A} = \begin{pmatrix} \mathbf{0} & \omega^2\mathbf{1} - \beta\mathbf{Z} \\ -\mathbf{1} & -\beta\mathbf{1} \end{pmatrix}, \quad \mathbf{B} = \begin{pmatrix} \mathbf{0} & \mathbf{0} \\ \mathbf{0} & q\,\boldsymbol{\Omega} \end{pmatrix}. \tag{A2}$$

The solution of Eq. (A1) can be found from general procedures for linear FPEs, as those presented, e.g., in Ref. [43]. Actually, it follows that W must be a Gaussian,

$$W(\vec{\Gamma},t) = \frac{\exp\left\{-\frac{1}{2}(\vec{\Gamma}-\vec{s})^{\mathrm{T}}\cdot\mathbf{S}^{-1}\cdot(\vec{\Gamma}-\vec{s})\right\}}{(2\pi)^3(\det\mathbf{S})^{1/2}}, \tag{A3}$$

where $\vec{s}$ and $\mathbf{S}$ are functions of time that can be obtained as solutions of the equations $d\vec{s}/dt = \mathbf{A}\cdot\vec{s}$ and $d\mathbf{S}/dt = -2\mathbf{s} + \mathbf{A}\cdot\mathbf{S} + \mathbf{S}\cdot\mathbf{A}^{\mathrm{T}}$, subjected to the initial conditions $\vec{s}\,(0) = \vec{\Gamma}\,(0)$ and $\mathbf{S}\,(0) = \mathbf{0}$, respectively. Thus, we have

$$\vec{s} = \exp\{\mathbf{A}t\}\cdot\vec{\Gamma}\,(0) \tag{A4}$$

and

$$\mathbf{S} = -2\int_0^t d\xi\,\exp\{\mathbf{A}(\xi-t)\}\cdot\mathbf{B}\cdot\exp\{\mathbf{A}^{\mathrm{T}}(\xi-t)\}. \tag{A5}$$

By noticing that $\mathbf{Z}^a = 0$, for any integer $a > 1$, we obtain the following expression for the exponential matrix:

$$\exp\{\mathbf{A}t\} = \begin{pmatrix} \Upsilon_{11}(t)\,\mathbf{1} & \Upsilon_{12}(t)\,\mathbf{1} \\ \Upsilon_{21}(t)\,\mathbf{1} & \Upsilon_{22}(t)\,\mathbf{1} \end{pmatrix} + \begin{pmatrix} \Xi_{11}(t)\,\mathbf{Z} & \Xi_{12}(t)\,\mathbf{Z} \\ \Xi_{21}(t)\,\mathbf{Z} & \Xi_{22}(t)\,\mathbf{Z} \end{pmatrix}, \tag{A6}$$

where the explicit form of the functions $\Upsilon_{ij}(t)$ and $\Xi_{ij}(t)$ has been obtained but will not be presented here for brevity.

Then, we replace Eq. (A6) into Eqs. (A4) and (A5), and return to the description in terms of the state vectors $\vec{X}$ and $\vec{U}$, by using the relations

$$\mathbf{H} = \begin{pmatrix} \omega^2\mathbf{1} - \beta\mathbf{Z} & \mathbf{0} \\ \mathbf{0} & \mathbf{1} \end{pmatrix}^{-1}\cdot\mathbf{S}\cdot\begin{pmatrix} (\omega^2\mathbf{1} - \beta\mathbf{Z})^{\mathrm{T}} & \mathbf{0} \\ \mathbf{0} & \mathbf{1} \end{pmatrix}^{-1} \tag{A7}$$

and

$$\begin{pmatrix} \vec{X} - \vec{X}_{\mathrm{d}} \\ \vec{U} - \vec{U}_{\mathrm{d}} \end{pmatrix} = \begin{pmatrix} \omega^2\mathbf{1} - \beta\mathbf{Z} & \mathbf{0} \\ \mathbf{0} & \mathbf{1} \end{pmatrix}^{-1}\cdot(\vec{\Gamma} - \vec{s}). \tag{A8}$$

This procedure yields Eq. (5) with the following explicit contributions. The covariance matrix $\mathbf{H}$ can be written as

$$\mathbf{H}(t) = \begin{pmatrix} \mathbf{P}(t) & \mathbf{R}(t) \\ \mathbf{R}^T(t) & \mathbf{Q}(t) \end{pmatrix}, \tag{A9}$$

where submatrices $\mathbf{P}$, $\mathbf{Q}$, and $\mathbf{R}$ read as

$$\mathbf{P} = 2q\int_0^t d\xi\,[\psi^2(\xi)\boldsymbol{\Omega} + \psi(\xi)\kappa(\xi)(\boldsymbol{\Omega}\cdot\mathbf{Z}^{\mathrm{T}} + \mathbf{Z}\cdot\boldsymbol{\Omega}) + \kappa^2(\xi)\mathbf{Z}\cdot\boldsymbol{\Omega}\cdot\mathbf{Z}^{\mathrm{T}}], \tag{A10}$$

$$\mathbf{Q} = 2q\int_0^t d\xi\,[\phi^2(\xi)\boldsymbol{\Omega} + \phi(\xi)\lambda(\xi)(\boldsymbol{\Omega}\cdot\mathbf{Z}^{\mathrm{T}} + \mathbf{Z}\cdot\boldsymbol{\Omega}) + \lambda^2(\xi)\mathbf{Z}\cdot\boldsymbol{\Omega}\cdot\mathbf{Z}^{\mathrm{T}}], \tag{A11}$$

$$\mathbf{R} = 2q\int_0^t d\xi\,[\psi(\xi)\phi(\xi)\boldsymbol{\Omega} + \phi(\xi)\kappa(\xi)\mathbf{Z}\cdot\boldsymbol{\Omega} + \psi(\xi)\lambda(\xi)\boldsymbol{\Omega}\cdot\mathbf{Z}^{\mathrm{T}} + \lambda(\xi)\kappa(\xi)\mathbf{Z}\cdot\boldsymbol{\Omega}\cdot\mathbf{Z}^{\mathrm{T}}]. \tag{A12}$$

In turn, the functions of time ψ and κ have the explicit form

$$\psi(t) = \frac{1}{\mu_1 - \mu_2}(e^{\mu_1 t} - e^{\mu_2 t}), \tag{A13}$$

$$\kappa(t) = \chi\left[t\zeta(t) - \frac{2}{\mu_1 - \mu_2}\psi(t)\right], \tag{A14}$$

with $\zeta(t) = (e^{\mu_1 t} + e^{\mu_2 t})/(\mu_1 - \mu_2)$, $\mu_{1,2} = -\beta/2 \pm \sqrt{(\beta/2)^2 - \omega^2}$, and $\chi = (\mu_1 + \mu_2)/(\mu_2 - \mu_1)$. Functions ϕ and λ can be obtained by derivation, namely, $\phi(t) = d\psi/dt$ and $\lambda(t) = d\kappa/dt$.

Finally, the components of $\vec{X}_{\rm d}$ read as

$$X_{\rm d,1}(t) = \frac{1}{\mu_1-\mu_2}[(\mu_1 X_{0,1} - U_{0,1})e^{\mu_2 t} - (\mu_2 X_{0,1} - U_{0,1})e^{\mu_1 t}], \tag{A15}$$

$$X_{\rm d,2}(t) = \frac{1}{\mu_1-\mu_2}[(\mu_1 X_{0,2} - U_{0,2})e^{\mu_2 t} - (\mu_2 X_{0,2} - U_{0,2})e^{\mu_1 t}], \tag{A16}$$

$$X_{\rm d,3}(t) = \frac{1}{\mu_1-\mu_2}[(\mu_1 X_{0,3} - U_{0,3})e^{\mu_2 t} - (\mu_2 X_{0,3} - U_{0,3})e^{\mu_1 t}] + \frac{\dot{\gamma}\chi}{\mu_1-\mu_2}\left\{e^{\mu_1 t}\left[X_{0,1} - \left(t - \frac{2}{\mu_1-\mu_2}\right)(\mu_2 X_{0,1} - U_{0,1})\right]\right.$$
$$\left. + e^{\mu_2 t}\left[X_{0,1} - \left(t - \frac{2}{\mu_2-\mu_1}\right)(\mu_1 X_{0,1} - U_{0,1})\right]\right\} - \chi\left(\frac{1-e^{\mu_1 t}}{\mu_1} - \frac{1-e^{\mu_2 t}}{\mu_2}\right) v_3(\vec{r}_0); \tag{A17}$$

while the components of $\vec{U}_{\rm d}$ can be obtained from derivation of the previous expressions $\vec{U}_{\rm d} = d\vec{X}_{\rm d}/dt$.

APPENDIX B: MEMORY KERNELS FOR THE FREQUENCY DEPENDENT DRAG FORCES

Functions $\tilde{\beta}$ and $\tilde{\tilde{\beta}}$ appearing in Eq. (17) have the explicit form

$$\tilde{\beta}(\omega) = \frac{2\beta\tilde{\alpha}^2}{-\omega^2\tau_{\rm s}^2 A + 2\tilde{\alpha}^2 B}\left[\left(1+\tilde{\alpha}+\frac{1}{9}\tilde{\alpha}^2\right)B + \frac{1}{9}\omega^2\tau_{\rm s}^2 A\right] \tag{B1}$$

and

$$\tilde{\tilde{\beta}}(\omega) = \frac{2\beta\tilde{\alpha}^2}{-\omega^2\tau_{\rm s}^2 A + 2\tilde{\alpha}^2 B} B\left(1+\tilde{\alpha}+\frac{1}{3}\tilde{\alpha}^2\right), \tag{B2}$$

respectively. In these expressions, β must be considered as the Stokes limit of the drag coefficient for stick boundary conditions $\beta = 6\pi\eta R$, where η is the dynamic viscosity. In addition, we have $\tilde{\alpha} = (-i\omega\tau_{\rm f})^{1/2}$ with $\mathrm{Re}\{\tilde{\alpha}\} > 0$; $A = 1 + \tilde{\alpha} + \tilde{\alpha}^2/3$; and $B = 1 + i\omega\tau_{\rm s} - \omega^2\tau_{\rm s}^2/3$.

The auxiliary function $\beta_{\rm slip}$ appearing in Eq. (28) is defined by

$$\beta_{\rm slip}(\omega) = \frac{\beta}{3}\frac{(1+\tilde{\lambda})(18+18\tilde{\alpha}+3\tilde{\alpha}^2+\tilde{\alpha}^3)+4(1+\tilde{\alpha})\tilde{\lambda}^2}{(2+2\tilde{\lambda}+\tilde{\lambda}^2)(3+\tilde{\alpha})+2(1+\tilde{\alpha})\tilde{\lambda}^2/\tilde{\alpha}^2}, \tag{B3}$$

where $\beta = 4\pi\eta R$ is the Stokes limit of the drag coefficient for slip boundary conditions and $\tilde{\lambda} = \omega\tau_{\rm s}/(-1-i\omega\tau_{\rm d})^{1/2}$.

The definition and physical meaning of the characteristic times $\tau_{\rm s}$, $\tau_{\rm f}$, and $\tau_{\rm d}$ appearing in Eqs. (B1)–(B3) are discussed in the main text.

[1] J. Keizer, *Statistical Thermodynamics of Nonequilibrium Processes* (Springer, New York, 1987).
[2] R. Kubo, M. Toda, and N. Hashitsume, *Statistical Physics II. Nonequilibrium Statistical Mechanics*, 2nd ed. (Springer, Berlin, 1991).
[3] J. M. Ortiz de Zárate and J. V. Sengers, *Hydrodynamic Fluctuations in Fluids and Fluid Mixtures* (Elsevier, Amsterdam, 2006).
[4] G. Lebon, D. Jou, and J. Casas-Vázquez, *Understanding Non-equilibrium Thermodynamics* (Springer, Berlin, 2008).
[5] S. R. de Groot and P. Mazur, *Non-Equilibrium Thermodynamics* (Dover, New York, 1984).
[6] I. Santamaría-Holek, R. Lugo-Frías, R. F. Rodríguez, and A. Gadomski, in *Thermodynamics-Physical Chemistry of Aqueous Systems*, edited by J. C. Moreno Piraján (InTech, Croatia, 2011).
[7] M. C. Marchetti and J. W. Dufty, J. Stat. Phys. **32**, 255 (1983).
[8] R. F. Rodríguez, E. Salinas-Rodríguez, and J. W. Dufty, J. Stat. Phys. **32**, 279 (1983).
[9] G. Subramanian and J. F. Brady, Phys. A (Amsterdam) **334**, 343 (2004).
[10] Y. Drossinos and M. W. Reeks, Phys. Rev. E **71**, 031113 (2005).
[11] I. Santamaría-Holek, D. Reguera, and J. M. Rubí, Phys. Rev. E **63**, 051106 (2001).
[12] D. Reguera, J. M. Rubí, and J. M. G. Vilar, J. Chem. Phys. B **109**, 21502 (2005).
[13] I. Santamaría-Holek, J. M. Rubí, and A. Pérez-Madrid, New J. Phys. **7**, 35 (2005).
[14] V. Breedveld, D. van den Ende, A. Tripathi, and A. Acrivos, J. Fluid Mech. **375**, 297 (1998).
[15] D. J. Pine, J. P. Gollub, J. F. Brady, and A. M. Leshansky, Nature (London) **438**, 997 (2005).
[16] J. S. Guasto, A. S. Ross, and J. P. Gollub, Phys. Rev. E **81**, 061401 (2010).
[17] H. Orihara and Y. Takikawa, Phys. Rev. E **84**, 061120 (2011).
[18] S. Sarman, D. J. Evans, and A. Baranyai, Phys. Rev. A **46**, 893 (1992).
[19] N. T. N. Phung, J. F. Brady, and G. Bossis, J. Fluid Mech. **313**, 181 (1996).
[20] D. R. Foss and J. F. Brady, J. Fluid Mech. **407**, 167 (2000).
[21] H. J. M. Hanley and D. J. Evans, J. Chem. Phys. **76**, 3225 (1982).
[22] A. Ahmed and R. J. Sadus, AIChE J. **57**, 250 (2011).
[23] G. Marcelli, B. D. Todd, and R. J. Sadus, Phys. Rev. E **63**, 021204 (2001).

[24] C. Van den Broeck, J. M. Sancho, and M. San Miguel, Phys. A (Amsterdam) **116**, 448 (1982).
[25] A. Ziehl, J. Bammert, L. Holzer, C. Wagner, and W. Zimmermann, Phys. Rev. Lett. **103**, 230602 (2009).
[26] L. Holzer, J. Bammert, R. Rzehak, and W. Zimmermann, Phys. Rev. E **81**, 041124 (2010).
[27] H. Híjar, J. Chem. Phys. **139**, 234903 (2013).
[28] H. J. H. Clercx and P. P. J. M. Schram, Phys. Rev. A **46**, 1942 (1992).
[29] T. Franosch, M. Grimm, M. Belushkin, F. M. Mor, G. Foffi, L. Forró, and S. Jenney, Nature (London) **478**, 85 (2011).
[30] D. Bedeaux and P. Mazur, Physica (Amsterdam) **78**, 505 (1974).
[31] P. Mazur and D. Bedeaux, Physica (Amsterdam) **76**, 235 (1974).
[32] V. Romero-Rochín, Phys. Rev. Lett. **94**, 130601 (2005).
[33] L. D. Landau and E. M. Lifshitz, *Theory of Elasticity*, 2nd revised ed. (Pergamon, London, 1970).
[34] N. Sandoval-Figueroa and V. Romero-Rochín, Phys. Rev. E **78**, 061129 (2008).
[35] M. Belushkin, R. G. Winkler, and G. Foffi, J. Phys. Chem. B **115**, 14263 (2011).
[36] G. G. Stokes, Trans. Cambridge Philos. Soc. **9**(part II), 8 (1851).
[37] R. Zwanzig and M. Bixon, Phys. Rev. A **2**, 2005 (1970).
[38] R. Zwanzig and M. Bixon, J. Fluid Mech. **69**, 21 (1975).
[39] H. Metiu, D. W. Oxtoby, and K. F. Freed, Phys. Rev. A **15**, 361 (1977).
[40] A. N. Guz, Int. Appl. Mech. **29**, 959 (1993).
[41] P. Español, Phys. A (Amsterdam) **214**, 185 (1995).
[42] B. U. Felderhof, J. Chem. Phys. **123**, 184903 (2005).
[43] J. K. G. Dhont, *An Introduction to Dynamics of Colloids* (Elsevier, Amsterdam, 2003).
[44] S. Chandrasekhar, Rev. Mod. Phys. **15**, 1 (1943).
[45] D. Frenkel and B. Smith, *Understanding Molecular Simulations: From Algorithms to Applications* (Academic, San Diego, 2002).
[46] A. Malevanets and R. Kapral, J. Chem. Phys. **110**, 8605 (1999).
[47] A. Malevanets and R. Kapral, J. Chem. Phys. **112**, 7260 (2000).
[48] R. Kapral, Adv. Chem. Phys. **140**, 89 (2008).
[49] G. Gompper, T. Ihle, D. M. Kroll, and R. G. Winkler, Multi-Particle Collision Dynamics: A Particle-Based Mesoscale Simulation Approach to the Hydrodynamics of Complex Fluids, in *Advanced Computer Simulation Approaches for Soft Matter Sciences III*, edited by C. Holm and K. Kremer (Springer, Berlin, Heidelberg, 2009).
[50] J. M. Yeomans, Phys. A (Amsterdam) **369**, 159 (2006).
[51] T. Ihle and D. M. Kroll, Phys. Rev. E **63**, 020201 (2001).
[52] T. Ihle and D. M. Kroll, Phys. Rev. E **67**, 066706 (2003).
[53] A. W. Lees and S. F. Edwards, J. Phys. C: Solid State Phys. **5**, 1921 (1972).
[54] H. Híjar and G. Sutmann, Phys. Rev. E **83**, 046708 (2011).
[55] C. C. Huang, G. Gompper, and R. G. Winkler, Phys. Rev. E **86**, 056711 (2012).
[56] J. Fernández and H. Híjar, Rev. Mex. Fis. **61**, 1 (2015).
[57] M. Hecht, J. Harting, T. Ihle, and H. J. Herrmann, Phys. Rev. E **72**, 011408 (2005).
[58] A. Erbas, R. Podgornik, and R. R. Netz, Eur. Phys. J. E **32**, 147 (2010).
[59] L. Holzer, Ph.D thesis, Universität Bayreuth, 2009.